# AN ANALYSIS OF THE RAPID PRESSURE-STRAIN CORRELATION IN COMPRESSIBLE SHEAR FLOW

**William D. Thacker**
Saint Louis University, St. Louis, MO 63156
thackerwd@slu.edu

**Sutanu Sarkar**
University of California at San Diego, La Jolla, CA 92093
sarkar@ucsd.edu

**Thomas B. Gatski**
NASA Langley Research Center, Hampton, VA 23681
t.b.gatski@larc.nasa.gov

## ABSTRACT

The influence of compressibility on the rapid pressure-strain rate correlation is investigated using the Green's function for the wave equation governing pressure fluctuations in compressible homogeneous shear flow. The solution for the Green's function is obtained as a combination of parabolic cylinder functions; it is oscillatory with monotonically increasing frequency and decreasing amplitude at large times, and anisotropic in wave-vector space. This Green's function, which depends explicitly on turbulent Mach number $M_t$ and gradient Mach number $M_g$, provides a means for analyzing the influence of these two compressibility parameters on the rapid pressure term. Assuming a form for the temporal decorrelation of velocity fluctuations brought about by the turbulence, the rapid pressure-strain rate tensor is expressed exactly in terms of the energy spectrum tensor and the time integral of the Green's function times a decaying exponential. A model for the energy spectrum tensor, linear in Reynolds stress anisotropies and in mean shear, is assumed for closure. The expression for the rapid pressure-strain correlation is evaluated using parameters applicable to a mixing layer and a boundary layer. It is found that, for the same range of $M_t$, there is a large reduction of the pressure-strain correlation in the mixing layer but not in the boundary layer. This result is linked with the observation that $M_g/M_t$ is considerably larger for the mixing layer than for the boundary layer.

## INTRODUCTION

The influence of compressibility on turbulence is an important issue for supersonic and hypersonic flight. One of the most pronounced effects of compressibility is the suppression of the growth rate and turbulence levels in a supersonic shear layer that have been traced to a reduced turbulence production and ultimately to a reduced pressure-strain correlation(Sarkar 1996; Vreman, Sandam, and Luo 1996; Simone, Coleman, and Cambon 1997; Freund, Lele, and Moin 2000; Pantano and Sarkar 2002). On the other hand, in a boundary layer with similar mean Mach number, such intrinsic compressibility effects are found to be weak. Two local Mach numbers are the turbulent Mach number $M_t = u_e^*/c$, and the gradient Mach number $M_g = \mathcal{S}^* l_e^*/c^*$. Here, $u_e^*$ is the rms velocity fluctuation, $\mathcal{S}^*$ is the mean velocity gradient and $l_e^*$ is the transverse integral length scale. In a turbulent boundary layer, $M_g$ is approximately half $M_t$, while in a shear layer $M_g$ is significantly greater than $M_t$. It has been argued (Sarkar 1995) that the difference in $M_g$ may be responsible for the enhanced compressibility effects observed in free shear layers relative to boundary layers. The objectives of this work are to quantify the influence of the parameters $M_t$ and $M_g$ on the pressure-strain rate correlation, $\Pi_{ij}$, using an analysis of the equation governing pressure fluctuations, and to explore potential differences between the shear layer and the boundary layer.

## FLUCTUATING PRESSURE FIELD

In a compressible flow, the pressure is governed by a wave equation and fluctuations propagate at the speed of sound. The fluctuating pressure at each point $P$ of a compressible flow is influenced only by the backwards sonic cone of $P$, consisting of all points in the past of $P$ which can reach $P$ by a signal propagating at the speed of sound. With increasing Mach number, the properties of this cone are altered and so must be the pressure-strain correlation. The shear-induced distortion of the path of pressure waves in high-speed flow is best understood within the context of geometric acoustics. For short wavelengths, the moving wave-vector $\boldsymbol{\mathcal{K}}$ can be used to construct rays (Landau and Lifshitz 1987) along which the pressure fluctuations propagate. The governing equations (Landau and Lifshitz 1987) for these rays are then

$$\frac{dx_i}{dt} = \frac{\mathcal{K}_i}{|\boldsymbol{\mathcal{K}}|} + M_g \tilde{u}_i \tag{1}$$

Since the rays are everywhere normal to the wavefronts, the tangent at any point along these rays is in the same direction as the direction of propagation. Figure 1(b) is a schematic in physical space of such rays emanating from a source in a homogeneous shear flow ($\mathcal{K}_3 = x_3 = 0$) with $M_g = 1$. In this moving medium, the propagation is in the direction of

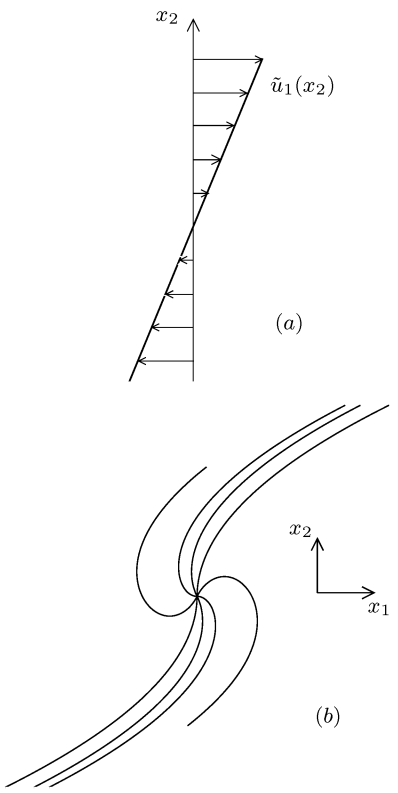


Figure 1: Sketch of: (a) homogeneous shear mean velocity profile; (b) ray trajectories in homogeneous shear flow ($M_g = 1$). Rays emanating from source at initial angular spacings of $\pi/4$.

the moving wave-vector times the speed of sound plus the velocity of the mean flow ($\lambda_{ij}x_j$). The figure clearly illustrates the significant effect the mean shear has on the propagation of pressure fluctuations; a distortion that increases with increasing $M_g$. The distortion is similar to that obtained by Papamoschou (1993) who applied ray theory to the mixing layer with hyperbolic tangent mean profile. It has been shown by Papamoschou (1993) and Papamoschou and Lele (1993) that communication of pressure signals in a mixing layer is hindered in the streamwise direction. Although ray theory gives this important qualitative implication, it is not sufficient to make analytical progress in linking $M_g$ to the pressure-strain correlation. Further progress is provided by the Green's function approach as explained below.

Pressure fluctuations in uniform shear flow satisfy the following (nondimensional) wave equation,

$$\left[\left(M_t\frac{\partial}{\partial t}+M_g\tilde{u}_j\frac{\partial}{\partial x_j}\right)^2\frac{\partial^2}{\partial x_j\partial x_j}\right]p' = f' \ , \tag{2}$$

where, only terms involving the mean shear are retained in $f'$ given our interest in the rapid $\Pi_{ij}$. Equation (2) shows that both $M_t$ and $M_g$ influence $p'$. After the introduction of a Green's function, the formal solution of Eq. (2) is then given in wave-vector space by

$$\hat{p}(\mathbf{k},t) = \int_0^t dt'\widehat{G}(\mathbf{k},t-t')\hat{f}(\mathbf{k},t') \ . \tag{3}$$

The first step in the derivation of the Green's function is to consider a moving wave-vector transform of $\widetilde{G}(\mathbf{k},t)$, that is

$$G(\mathbf{x},t) = \frac{1}{(2\pi)^3}\int d^3\mathbf{k}e^{\imath\boldsymbol{\mathcal{K}}(\mathbf{k},t)\cdot\mathbf{x}}\widetilde{G}(\mathbf{k},t) \ . \tag{4}$$

The moving wave-vector $\boldsymbol{\mathcal{K}}(\mathbf{k},t)$ given in Eq. (4), defined in terms of the (fixed) wave-vector $\mathbf{k}$ as

$$[\mathcal{K}_1,\ \mathcal{K}_2,\ \mathcal{K}_3] = \left[k_1,\ k_2-\frac{M_g}{M_t}k_1t,\ k_3\right] , \tag{5}$$

corresponds to a coordinate transformation from the fixed frame to one moving with the mean shear flow. Equation (5) allows the wave equation for $\widetilde{G}(\mathbf{k},t)$ to be written as

$$\left[M_t^2\frac{\partial^2}{\partial t^2} + \left(\frac{M_gk_1}{M_t}\right)^2\left(t-\frac{k_2}{k_1}\frac{M_t}{M_g}\right)^2\left(k_1^2+k_3^2\right)\right]\widetilde{G}(\mathbf{k},t) = \delta(t) \ , \tag{6}$$

where

$$\mathcal{K}^2 = (k_1^2+k_2^2+k_3^2) - 2k_2\left(\frac{M_g}{M_t}k_1t\right) + \left(\frac{M_g}{M_t}k_1t\right)^2 \tag{7}$$

has been used. The limiting case of shear-free flow ($M_g = 0, \mathcal{K}_i\mathcal{K}_i = k_ik_i$) has been studied previously by Pantano and Sarkar (2002), who determined the corresponding shear-free Green's function $\widetilde{G}_{sf}(\mathbf{k},t)$ which, in the notation used here, can be written as

$$\widetilde{G}_{sf}(k,t) = \frac{\mathcal{H}(t)}{M_tk}\sin\left(kt/M_t\right) \ , \tag{8}$$

where $k^2 = k_ik_i$, and $\mathcal{H}(t)$ is the Heaviside function. Fortunately, as shown below, it is also possible to obtain the solution to Eq. (6) for $\widetilde{G}(\mathbf{k},t)$ in the homogeneous shear case.

For $t \neq 0$, Eq. (6) can be transformed into an equation having the form

$$\frac{d^2\widetilde{G}}{d\xi^2} + \left(\frac{\xi^2}{4}-a\right)\widetilde{G} = 0 \ , \tag{9}$$

where

$$\xi(\mathbf{k},t) = \left(\frac{2M_g|k_1|}{M_t^2}\right)^{1/2}\left(t-\frac{k_2}{k_1}\frac{M_t}{M_g}\right) \tag{10a}$$

$$a = -\left(\frac{k_1^2+k_3^2}{2M_g|k_1|}\right) \ . \tag{10b}$$

The solution of this equation can be written in terms of parabolic cylinder functions (see Sec. 19.17, p. 692 of Abramowitz and Stegun (1970)) as follows,

$$\widetilde{G}(\xi) = c_1W_1(a,\xi) + c_2W_2(a,\xi) \ , \tag{11a}$$

where

$$W_1(a,\xi) = W(a,\xi) \quad \text{and} \quad W_2(a,\xi) = W(a,-\xi) \tag{11b}$$

are two linear independent solutions of Eq. (9) with Wronskian equal to unity and $W(a,\xi)$ defined by Abramowitz and Stegun (1970). Since $a < 0$, the function $W(a,\xi)$ is oscillatory for all $\xi$ and the factor $\sqrt{\xi^2/4-a}$ plays the role of a (local) frequency. The coefficients $c_1$ and $c_2$ are determined from the conditions imposed on the solution at $t = 0$, and then the result in the

moving wave-vector form is transformed to the required fixed-wave number Green's function $\widehat{G}(\mathbf{k},t)$. After some algebra, the *final* expression for the Green's function is

$$\widehat{G}(\mathbf{k},t) = \frac{\mathcal{H}(t)}{M_t(2M_g|k_1|)^{1/2}}[W_1(a,\eta_0)W_2(a,\eta) - W_2(a,\eta_0)W_1(a,\eta)] \quad (12)$$

with $\eta_0$ and $\eta$ defined by

$$\eta_0(k_1,k_2,k_3) = \left(\frac{2|k_1|}{M_g}\right)^{1/2}\frac{k_2}{k_1} \quad (13a)$$

$$\eta(k_1,k_2,k_3;t) = \frac{(2M_g|k_1|)^{1/2}}{M_t}\left(t+\frac{k_2}{k_1}\frac{M_t}{M_g}\right) . \quad (13b)$$

Figure 2, an example of the time evolution of the Green's function, shows four cases with different wave number orientation but the same magnitude, $k = 2.2$. The orientation is given by the azimuthal angle, $\phi$, and the polar angle, $\theta$, so that the streamwise $k_1$, cross-stream $k_2$, and spanwise $k_3$ wavenumbers are given by $k_1 = k\sin\theta\cos\phi$, $k_2 = k\sin\theta\sin\phi$, and $k_3 = k\cos\theta$. Note that $\theta = \pi/2$ corresponds to the $k_1 - k_2$ plane which is the plane of shear. For $\theta = 0$ and for $\phi = \pi/2, 3\pi/2$, $k_1 = 0$ and the Green's function $\widehat{G}$ for the homogeneous shear case reduces to the shear-free Green's function; otherwise the angle $\phi$ applies over the range $(0, 2\pi)$. For this example, the compressibility related parameters take the values $M_t = 0.2$ and $M_g = 1.0$. The four cases in Fig. 2 corresponding to $\phi = \pi/12$, $\pi/2$, $7\pi/12$, and $2\pi/3$ and in the shear plane, $\theta = \pi/2$ ($k_3 = 0$), characterize four different types of evolution. In all cases, except $\phi = \pi/2$, the damped oscillations of $\widehat{G}$ vanish at sufficiently long times ($t > 20$). If the function $\eta$ has no zero points ($\phi = \pi/12$), the temporal evolution of $\widehat{G}$ is simply a damped oscillation with increasing frequency and decaying amplitude as shown in Figure 2(a).

The shear-free Green's function $\widehat{G}_{sf}$ is shown in Fig. 2(b). This corresponds to the anisotropic Green's function $\widehat{G}$ at $k_1 = 0$ ($\phi = \pi/2$). A comparison with Figs. 2(a), (c) and (d) clearly shows the strong anisotropic behavior of $\widehat{G}$, and suggests that only the early transient behavior of $\widehat{G}$ at these other locations is similar to the shear-free function $\widehat{G}_{sf}$.

Figure 2(c) shows the effect on the evolution of $\widehat{G}$ when the function $\eta$ has a zero at some time $t$. At these locations, the frequency is a minimum and is given by $\sqrt{|a|}$. For example, at $\phi = 7\pi/12$, $\eta = 0$ when $t = (M_t/M_g)\cot(\pi/12) = 0.746$, the figure shows the effect on both the amplitude and local frequency ($\sqrt{k\cos(5\pi/12)/(2Mg)}$) of the $\widehat{G}$ oscillation. In this example, $\widehat{G} < 0$ in the vicinity of the critical point. The amplitude increases in magnitude to make $\widehat{G}$ more negative, and the frequency decreases significantly. As time continues to increase, the behavior of the Green's function oscillation returns to a more regular form characterized by a decrease in amplitude with an increase in frequency.

An increase in the angle $\phi$ further highlights the highly anisotropic character of the Green's function. Figure 2(d) shows the temporal evolution at $\phi = 2\pi/3$. At this location, the $\eta = 0$ condition occurs nearer to the initial state at $t = (M_t/M_g)\cot(\pi/6) = 0.346$. In this example $\widehat{G} > 0$ in the vicinity of the critical point, and the amplitude increases in magnitude to make $\widehat{G}$ more positive. In contrast with Fig. 2(c), the frequency decrease at $\phi = 2\pi/3$ is not as significant as the decrease at $\phi = 7\pi/12$. Note that initial amplitude variations at different angles $\phi$ are related to the fact that the anisotropic Green's function $\widehat{G}(\mathbf{k},t)$ is proportional to $|k_1|^{-1/2}$ (see Eq. (12)) where $k_1 = k\cos\phi$ in the $(k_1,k_2)$ plane.

## THE RAPID PRESSURE-STRAIN CORRELATION

The rapid part of $\Pi_{ij}$ can be related to the correlation,

$$\left\langle \hat{u}_i(\mathbf{k},t')\hat{u}_j(-\mathbf{k},t)\right\rangle = e^{-(t-t')/\tau_I}\delta^3(\mathbf{0})E_{ij}(\mathbf{k},t) , \quad (14)$$

where $E_{ij}$ is the energy spectrum tensor that is modeled by an expression linear in the Reynolds stress anisotropies (Shih, Reynolds, and Mansour 1990). An exponential temporal decorrelation ($t' < t$), with decorrelation time $\tau_I$, has been assumed (Pantano and Sarkar 2002). The pressure-strain rate correlation can then be expressed exactly in terms of the energy spectrum tensor and the Green's function as the following integral in wave-vector space,

$$\Pi_{ij} = 2\overline{\rho}\left(\frac{M_g}{M_t}\right)\int_0^\infty dk\int_0^\pi \sin\theta d\theta\int_0^{2\pi} d\phi R(k,\theta,\phi;\tau_I) \times k_l\lambda_{ln}\left[E_{ni}(k,\theta,\phi)k_j + E_{nj}(k,\theta,\phi)k_i\right] , \quad (15a)$$

where $\lambda_{ln}$ ($= \delta_{l1}\delta_{n2}$ here) is the nondimensionalized velocity gradient tensor, and

$$R(k,\theta,\phi;\tau_I) = k^2\int_0^\infty \widehat{G}(\mathbf{k},\tau)e^{-\tau/\tau_I}d\tau . \quad (15b)$$

For incompressible flows, the factor $R(k,\theta,\phi)$ is not present in Eq. (15a), and for shear-free compressible flows it is given by

$$R(k,\theta,\phi;\tau_I) = \left(1+\frac{M_t^2}{\tau_I^2k^2}\right)^{-1} , \quad (16)$$

where Eq. (8) has been used. In order to complete the modeling of the pressure-strain rate correlation, a suitable representation for the energy spectrum tensor $E_{ij}$ is needed.

Current incompressible models for the pressure-strain rate correlation, such as the Launder Reece and Rodi (LRR) model (Launder, Reece, and Rodi 1975), are based on $E_{ij}$ representations that are parameterized by terms linear in the second velocity moment anisotropy,

$$b_{ij} \equiv \frac{\left\langle u_i''u_j''\right\rangle}{2K} - \frac{\delta_{ij}}{3} , \quad (17)$$

where $K = \left\langle u_i''u_i''\right\rangle/2$. Such a (linear) representation for $E_{ij}(\mathbf{k};\mathbf{b})$ can be expressed in terms of the basis set $\delta_{ij}$, $\hat{k}_i\hat{k}_j$, $b_{ij}$, and $(b_{in}\hat{k}_n\hat{k}_j + \hat{k}_i\hat{k}_nb_{nj})$, with $\hat{k}_i = k_i/k$. When applied against the conditions that the trace of the second-moment spectrum tensor $E_{ij}$ is proportional to the (isotropic) energy spectral density $E(k)$ ($E_{ii} = E(k)/2\pi k^2$) and continuity $k_iE_{ij} = 0$, this four-term representation can be written as

$$\begin{aligned} E_{ij}(\mathbf{k};\mathbf{b}) &= \frac{E(k)}{4\pi k^2}\left(\delta_{ij} - \hat{k}_i\hat{k}_j\right) \\ &+ \frac{E_a(k)}{8\pi k^2}\left(\hat{k}_nb_{nm}\hat{k}_m\right)\left(\delta_{ij} + \hat{k}_i\hat{k}_j\right) \\ &+ \frac{E_a(k)}{4\pi k^2}\left[b_{ij} - \left(b_{in}\hat{k}_n\hat{k}_j + \hat{k}_i\hat{k}_nb_{nj}\right)\right] , \end{aligned} \quad (18)$$

where the expansion coefficient $E_a(k)$ is the anisotropic energy spectral density.

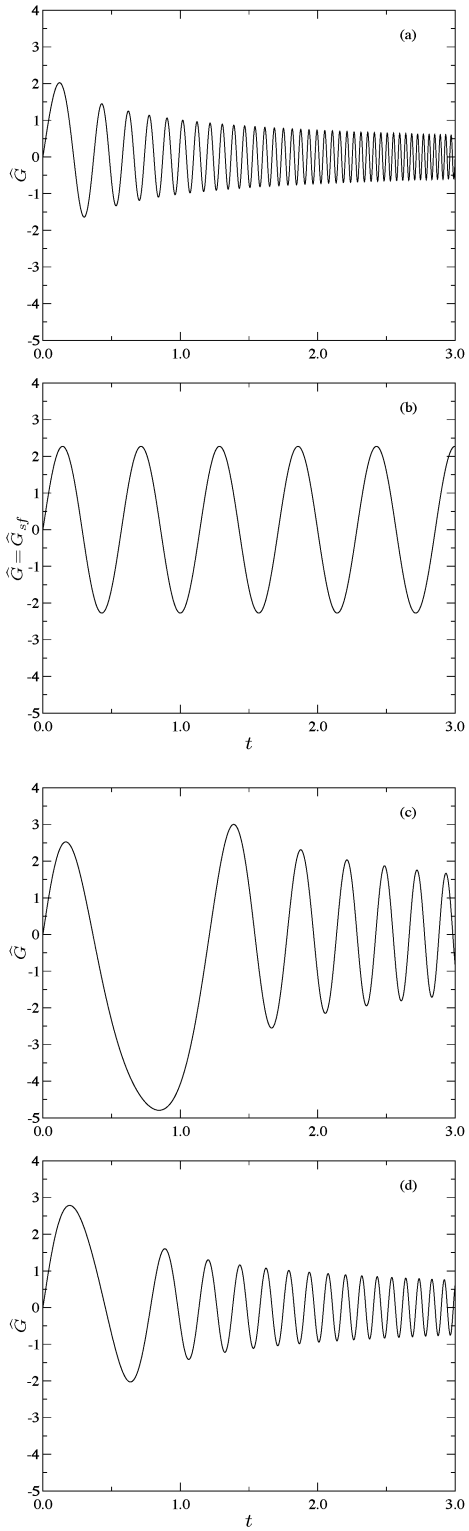


Figure 2: Time evolution of fixed wave-vector Green's functions $\widehat{G}$ at $M_t = 0.2$ and $M_g = 1.0$ with wave-vector at various values of the azimuthal angle $\phi$ on a circle of radius $k = 2.2$ in the shear plane $\theta = \pi/2$ ($k_3 = 0$): (a) $\phi = \pi/12$, (b) $\phi = \pi/2$, (c) $\phi = 7\pi/12$, (d) $\phi = 2\pi/3$

Shih, Reynolds, and Mansour (1990) used an expression similar to Eq. (18) and an incompressible form of Eq. (15a) to obtain a closure model for the pressure-strain rate correlation that corresponded to the linear LRR model. In the incompressible case where the factor $R(k, \theta, \phi)$ is not present in Eq. (15a), exact forms for both $E(k)$ and $E_a(k)$ are not required in order to obtain a solution of Eq. (15a). Rather they are obtained from the conditions imposed by the integral relation between the Reynolds stress energy spectrum and the Reynolds stress anisotropy tensor

$$\int_0^\infty d^3\mathbf{k} E_{ij} = 2K\left(b_{ij} + \frac{\delta_{ij}}{3}\right) , \tag{19a}$$

that is,

$$\int_0^\infty E(k)dk = K \qquad \text{and} \qquad \int_0^\infty E_a(k)dk = 5K . \tag{19b}$$

In the compressible case, where the factor $R(k, \theta, \phi)$ is present in Eq. (15a), modeled forms for both $E(k)$ and $E_a(k)$ are required in order to evaluate the integral in Eq. (15a).

To summarize, Eq. (15a) is the final expression for the rapid pressure-strain correlation which, after assuming models for the isotropic and anisotropic spectra that are calibrated with inputs from DNS, is used in the next section to compute its components for various values of Mach numbers $M_t$ and $M_g$.

## COMPRESSIBILITY EFFECTS ON THE PRESSURE-STRAIN CORRELATION

In order to assess the influence of compressibility, $M_t$ and $M_g$, on the rapid part of the pressure-strain rate correlation in shear flows, consistent spectral models for both the isotropic, $E(k)$, and anisotropic, $E_a(k)$, energy spectral densities are required. The rapid part $\Pi_{ij}$ given in Eq. (15a) requires the energy spectrum tensor $E_{ij}$ given in Eq. (18) which is composed of the isotropic, $E(k)$, and anisotropic, $E_a(k)$, energy spectral densities. For the isotropic energy spectral density, the Von Karman spectrum is chosen and is given by, for example, by Pope (2000),

$$E(k) = C\varepsilon^{2/3}k^{-5/3}\left[\frac{kL}{[(kL)^2 + C_L]^{1/2}}\right]^{17/3} , \tag{20}$$

where $C = 1.5$ is the Kolmogorov constant, $\varepsilon$ is the isotropic dissipation rate associated with $K$, $L$ is the length scale defined as $K^{3/2}/\varepsilon$, and

$$C_L = \left[\frac{27}{55}\frac{\Gamma(\frac{3}{2})\Gamma(\frac{1}{3})}{\Gamma(\frac{5}{6})}C\right]^3 \approx 3.72 , \tag{21}$$

is a low wavenumber scaling coefficient extracted from the condition on the isotropic energy spectral density given in Eq. (19b) ($\Gamma(n)$ is the Gamma function). Here the low wavenumber behavior $E(k) \propto k^4$ is assumed. A model for the anisotropic energy spectral density $E_a(k)$ can be developed from an inertial range model proposed by (Lumley 1967) for the one-dimensional shear stress spectrum based on similarity considerations for pure shear flow ($\lambda_{12} = 1$). As with the isotropic energy spectral density distribution $E(k)$, a two-range model is also assumed for the anisotropic energy spectral density $E_a(k)$. It is assumed here that the isotropic and anisotropic energy spectral densities have the same low-wavenumber behavior. This leads to a two-range model for

| Flow | $\frac{M_g}{M_t}$ | $\frac{L_2}{L}$ | $\frac{SK}{\epsilon}$ | $\frac{\tau_I u}{L_2}$ | $b_{11}$ | $b_{22}$ | $b_{12}$ |
|---|---|---|---|---|---|---|---|
| ML | 2.5 | 0.6 | 5.89 | 0.6 | 0.15 | -0.10 | -0.13 |
| BL | 0.55 | 0.14 | 5.56 | 1.5 | 0.18 | -0.14 | -0.14 |

Table 1: Parameters held constant in the mixing layer (ML) and boundary layer (BL) cases of the pressure-strain rate computations. Here $L_2$ is the transverse integral scale, $L = K^{3/2}/\epsilon$ with $K$ the turbulent kinetic energy and $\epsilon$ the turbulent dissipation rate, $u = \sqrt{(2k)}$ is the velocity fluctuation, $\tau_I$ is the decorrelation time scale, and $b_{ij}$ denotes the Reynolds stress anisotropy tensor.

$E_a(k)$ given by

$$E_a(k) = C_a \left(\frac{M_g}{M_t}\right) \varepsilon^{1/3} k^{-7/3} \left[\frac{kL}{[(kL)^2 + C_{aL}]^{1/2}}\right]^{19/3}, \quad (22)$$

where the coefficients $C_a$ and $C_{aL}$ are determined as discussed below.

The implications of the analytical solution, Eq. (15a), for the rapid $\Pi_{ij}$ are now explored for two prototypical flows, the shear layer and the boundary layer, choosing a separate set of parameters to typify each flow. For each flow, the required parameters are as follows. $M_g$ and $M_t$ govern the Green's function response in spectral space, Eq. (12). The Von Karman spectrum, Eq. (20), used here as a model for $E(k)$, is parameterized by the length scale ratio, $L_2/L$. The anisotropic energy spectral density, $E_a(k)$, modeled by the two-range spectrum, Eq. (22), requires knowledge of the normal stress anisotropies $b_{11}$ and $b_{22}$, the length scale ratio $L_2/L$, and the time scale ratio $T_r$ $(= \mathcal{S}^* K^*/\varepsilon^*)$. The decorrelation time scale, $\tau_I$ in Eq. (14) is also required.

The parameters summarized in Table 1 are held constant and the pressure-strain correlation is calculated for the range $0 < M_t < 0.4$ for the mixing layer and the boundary layer. The upper value of $M_t$ corresponds to a mixing layer with convective Mach number $M_c \simeq 1$ and to a boundary layer with free stream Mach number, $M_\infty \simeq 4.5$, so that this study covers a wide range of speeds of interest. The mixing layer entries correspond to centerline values collected from the $M_c = 0.7$ DNS database of Pantano and Sarkar (2002). Implicit is the assumption, supported by DNS, that the parameters in Table 1 do not change substantially with Mach number. For the boundary layer, values from the log-layer ($y^+ \approx 94$) in the $M = 2.25$ database of Pirozzoli, Grasso, and Gatski (2004) are used to obtain the entries in Table 1. Both these flows are two-dimensional in the mean with the mean velocity gradient tensor $\lambda_{ln} = \lambda_{ln}\delta_{l1}\delta_{n2}$. In these flows, the ratio of $M_g/M_t$ is found from DNS results to be 2.5 for the mixing layer (Pantano and Sarkar 2002) and 0.55 for the boundary layer (Pirozzoli, Grasso, and Gatski 2004), a difference that will be seen to have remarkable consequence. From the DNS data for the mixing layer, the centerline mean density $\overline{\rho} \simeq 1$, and from the DNS data for the boundary layer, the log-layer ($y^+ \approx 94$) mean density $\overline{\rho} = 0.71$,

The behavior of the streamwise component, $\Pi_{11}$, in the boundary layer is shown in Fig. 3(a). Clearly, Fig. 3(a) shows that there is large reduction in the magnitude of $\Pi_{11}$, a factor of 3 at $M_t = 0.4$ (convective Mach number, $M_c \simeq 1$). This value is of the same order as the factor of 3.3 reduction at $M_c = 1$ inferred from the 'Langley experimental data' and the factor of 2.5 reduction observed in the $M_c = 1.1$ data

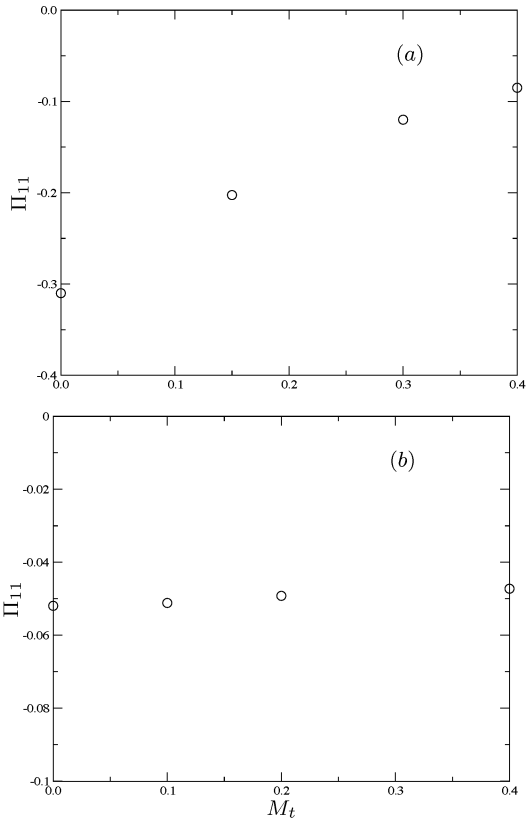


Figure 3: Variation of the streamwise component of the pressure-strain rate term as a function of turbulent Mach number: (a) Mixing layer, (b) Boundary layer.

of Pantano and Sarkar (2002). Clearly, there is only a small reduction in magnitude (less than 10%) of $\Pi_{11}$ in the boundary layer for the same range of $M_t$ (free stream Mach number up to 4.5), in accord with expectations. Compressibility effects on the other components of $\Pi_{ij}$ have also been examined. The magnitude of all normal components decrease substantially in the shear layer but show little change in the boundary layer.

## CONCLUSIONS

A systematic construction of the rapid pressure-strain rate correlation for compressible flow has been carried out starting from a convective wave equation that governs the behavior of the turbulent pressure fluctuations in homogeneous turbulence with a uniform velocity gradient. The formal solution of the fluctuating pressure equation in terms of the Green's function for the convective wave operator allows for the construction of the pressure-strain rate correlation in terms of the energy spectrum tensor. Unlike the incompressible case where details of the spectrum are not required, it is necessary here to introduce both the isotropic energy spectral density as well as a form for the anisotropic energy spectrum to explicitly obtain the pressure-strain correlation. Thus, functional forms derived for the rapid pressure-strain in the case of compressible flow are significantly altered relative to their incompressible counterparts where pressure fluctuations are assumed to satisfy a Poisson equation instead of a convective wave equation.

The case of homogeneous shear that is considered here has required the determination of the applicable Green's function,

found here to be a combination of parabolic cylinder functions. The Green's function is oscillatory in time with variable frequency and amplitude. Owing to mean shear, its behavior in wave-vector space is highly anisotropic; for instance, the amplitude and frequency of downstream propagating waves exhibit monotone decrease while, depending on the specifics, upstream propagating waves may exhibit strongly nonmonotone variation of frequency and amplitude. Once the Green's function is derived, closure of the rapid pressure-strain correlation is achieved through a spectral model that assumes Kolmogorov scaling of the isotropic energy spectrum in the inertial range and an anisotropic spectral density that is linear in the Reynolds stress anisotropies and in the mean shear.

The final expression for the rapid pressure-strain rate correlation in uniform shear flow involves two different measures of compressibility: the gradient Mach number, $M_g$, and the turbulent Mach number, $M_t$. It has been argued before that a reason for the much larger influence of compressibility on the pressure-strain correlation in a mixing layer compared to that in a boundary layer is that $M_g$ is larger in the former flow. In order to assess this claim, the pressure-strain correlation is evaluated for the mixing layer and the boundary layer using DNS data specific to each flow for fixing auxiliary quantities required in the calculation. It is found that when the turbulent Mach number varies in the range $0 < M_t < 0.4$ (equivalently, the convective Mach number varies as $0 < M_c < 1$) in the mixing layer calculations, the streamwise component of the pressure-strain rate correlation decreases substantially, almost a factor of three, in good agreement with the observed trend in DNS data and that inferred from experimental data on the thickness growth rate. For the same range of $M_t$, there is little change of the pressure-strain rate correlation in the boundary layer. Thus, the analysis performed here supports the important role of the gradient Mach number in determining the stabilizing effect of compressibility in shear flows.

Although the uniform shear flow solution is able to identify the essence of $M_g$ and $M_t$ effects in turbulent shear flows, it is recognized that the details would depend on specifics of each flow, for example, the flow-specific Green's function. The derivation of such Green's functions in future work would be useful. Furthermore, development of the analysis into a pressure-strain model for compressible flow applications and the testing of such a model could also be a topic for future work.

*

References


Abramowitz, M. and A. Stegun (1970). *Handbook of Mathematical Functions*. New York: Dover.

Freund, J. B., S. K. Lele, and P. Moin (2000). Compressibility effects in a turbulent annular mixing layer. part 1. turbulence and growth rate. *J. Fluid Mech. 421*, 229–267.

Landau, L. D. and E. M. Lifshitz (1987). *Fluid Mechanics*. Oxford: Pergamon.

Launder, B. E., G. J. Reece, and W. Rodi (1975). Progress in the development of a Reynolds-stress turbulence closure. *J. Fluid Mech. 68*, 537–566.

Lumley, J. L. (1967). Similarity and the turbulent energy spectrum. *Phys. Fluids 10*, 855–858.

Pantano, C. and S. Sarkar (2002). A study of compressibility effects in the high-speed turbulent shear layer using direct simulation. *J. Fluid Mech. 451*, 329–371.

Papamoschou, D. (1993). Zones of influence in the compressible shear layer. *Fluid Dyn. Res. 11*, 217–228.

Papamoschou, D. and S. K. Lele (1993). Vortex-induced disturbance field in a compressible shear layer. *Phys. Fluids A 5*, 1412–1419.

Pirozzoli, S., F. Grasso, and T. B. Gatski (2004). Direct numerical simulation and analysis of a spatially evolving supersonic turbulent boundary layer at $m = 2.25$. *Phys. Fluids 16*, 530–545.

Pope, S. B. (2000). *Turbulent Flows*. Cambridge: Cambridge University Press.

Sarkar, S. (1995). The stabilizing effect of compressibility in turbulent shear flow. *J. Fluid Mech. 282*, 163–186.

Sarkar, S. (1996, July). On density and pressure fluctuations in uniformly sheared compressible flow. In L. Fulachier, J. L. Lumley, and F. Anselmet (Eds.), *Proc. IUTAM Symp. on Variable Density Low-Speed Flows*.

Shih, T.-H., W. C. Reynolds, and N. N. Mansour (1990). A spectrum model for weakly anisotropic turbulence. *Phys. Fluids A 8*, 1500–1502.

Simone, A., G. N. Coleman, and C. Cambon (1997). The effect of compressibility on turbulent shear flow: a rapid-distortion-theory and direct-numerical-simulation study. *J. Fluid Mech. 330*, 307–338.

Vreman, A. W., N. D. Sandam, and K. L. Luo (1996). Compressible mixing layer growth rate and turbulence characteristics. *J. Fluid Mech. 320*, 235–258.